Applied Physics Letters

Field-induced migration of gold in molecular semiconductors

Cite as: Appl. Phys. Lett. **120**, 243503 (2022); https://doi.org/10.1063/5.0092224
Submitted: 22 March 2022 • Accepted: 03 June 2022 • Published Online: 15 June 2022

P. Riederer, M. Bouraoui and R. Kersting

AIP Publishing

Applied Physics Letters ARTICLE scitation.org/journal/apl

Field-induced migration of gold in molecular semiconductors

Cite as: Appl. Phys. Lett. **120**, 243503 (2022); doi: 10.1063/5.0092224
Submitted: 22 March 2022 · Accepted: 3 June 2022 ·
Published Online: 15 June 2022

P. Riederer, M. Bouraoui, and R. Kersting[a)]

AFFILIATIONS

Photonics and Optoelectronics Group, Faculty of Physics and Center for NanoScience (CeNS), Ludwig-Maximilians-Universität, Königinstr. 10, 80539 München, Germany

[a)]Author to whom correspondence should be addressed: roland.kersting@lmu.de

ABSTRACT

We report on the degradation of field-effect devices due to the migration of gold from injection contacts into the channel region. The experimental results are obtained by THz spectroscopy on devices with a migration distance of 50 nm. The dependence of the degradation on gate voltage, as well as the partial reversibility, indicates that degradation is caused by field-induced transport of gold ions. The transport is found to be thermally activated with an activation energy independent of the field strength, which suggests that lattice deformations of the molecular semiconductor support the migration of gold.

The application of molecular semiconductors for future electronic and optoelectronic devices requires excellent electronic performance as well as sufficient stability and reliability of the components.[1] In organic field-effect transistors (FETs), degradation can cause changes in threshold voltages,[2,3] hysteresis,[4] and increased contact resistances.[5,6] Extrinsic factors that diminish device reliability often arise from contaminations acquired during fabrication or due to indiffusion from the environment during device operation. Identified were, for instance, residues of water[7–9] and oxygen.[10,11] Less is known about the deterioration of the FETs' contacts[12] and the associated ingress of contact materials such as metals.[13,14] In this work, we show that gold contacts on molecular semiconductors are prone to field-induced migration, whereas molybdenum oxide (MoO_x) injection layers are much more stable. The electromigration of gold ions into the channel region reduces the density of mobile holes and increases the threshold voltage of field-effect devices.

Most organic FETs have a planar layout as illustrated in Fig. 1(a). Such structures offer a relatively large surface area for indiffusion of contaminants from the environment. Additionally, the transport toward the channel region is expedited by short distances, which rarely exceed 50 nm. In contrast, electromigration of metals from the source and drain contacts occurs along the channel length, which, in general, exceeds 1 μm. Thus, metal migration from the contacts can be expected to occur on longer timescales than indiffusion of contaminations from the surface. This makes definite studies of field-induced metal migration in FETs challenging. We, therefore, select devices as illustrated in Fig. 1(b), which provide much better access to ion migration of metals, because the transport distance toward the sensitive channel region is only on the order of 50 nm.

As illustrated in Fig. 1(b), the impact of metal defects on the density of mobile holes can be measured by THz electromodulation spectroscopy.[15] Without metal migration, a negative gate voltage V_g causes the injection of holes into the molecular semiconductor and their accumulation at the interface to the insulator. As long as the holes are mobile, the conductance of this sheet of charge carriers can be probed by THz spectroscopy, because the carriers' Drude response reduces the THz transmission. In contrast, charged defects do not respond to THz radiation. Such defects are formed by metals that migrate from the injection contacts into the molecular semiconductor. Because the total charge of mobile holes and charged defects depends only on the applied gate voltage V_g, the ingress of metal ions reduces the density of mobile holes, which leads to an increase in THz transmission.

Devices as illustrated in Fig. 1 are fabricated on foils of polyethylene naphthalate (PEN). The active area of the structure has a diameter of 5 mm, which is about twice the spot diameter of the incident THz radiation. The gate contact is a 6 nm thick chromium layer deposited by physical vapor deposition (PVD) onto the PEN foil. The insulator consists of a 300 nm thick parylene N layer, which is fabricated by chemical vapor deposition.[16] The organic semiconductor is a 50 nm thick layer of 2,7-dioctyl[1]benzothieno[3,2-b][1]benzothiophene (C_8-BTBT-C_8).[17] It is deposited by PVD at a base pressure of 10^{-7} mbar and at a rate of 0.2 Å/s. The injection layers consist either of (i) 2 nm

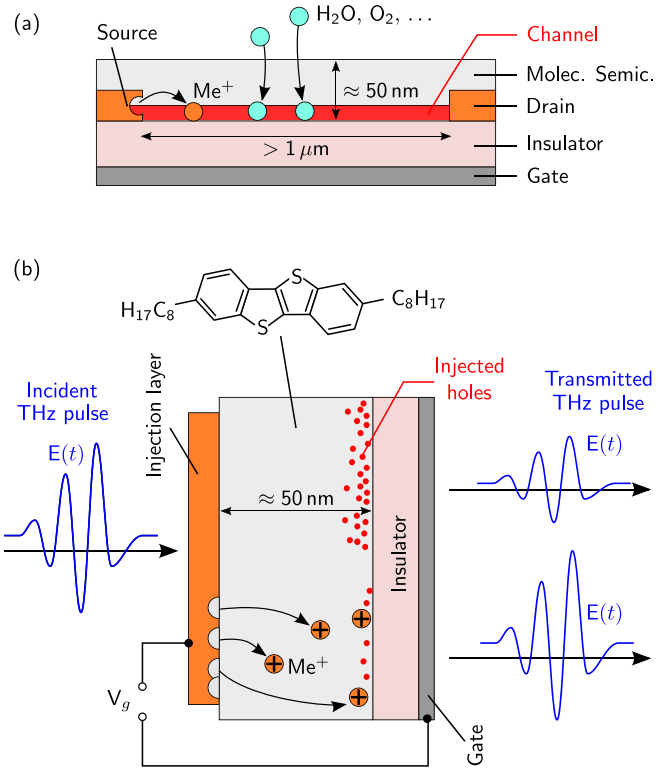

FIG. 1. Schematic and device dimensions of a typical organic FET (a). Illustration of the studied devices and of the measurement technique (b). Mobile holes reduce the transmission of the THz pulse by their Drude response. Electromigration of the injection layer material leads to positively charged metal defects within the semiconductor that reduce the density of mobile holes and, thus, enhance THz transmission.

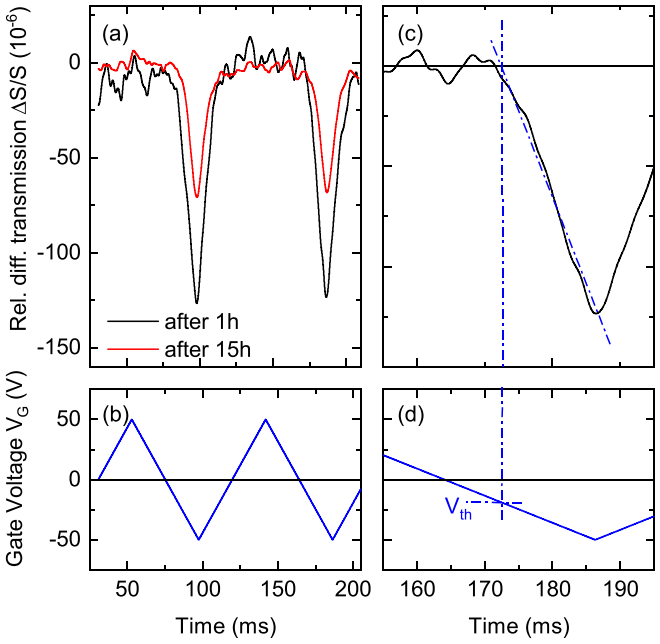

FIG. 2. Modulation of the THz transmission through a device with Au/Cr contacts. (a) Change of the relative differential THz transmission $\Delta S/S$ after 1 h and after 15 h of operation. (b) Applied gate voltage. (c) and (d) Magnifications of (a) and (b), respectively. The blue dashed-dotted lines indicate the procedure for deducing the threshold voltage V_{th}.

of gold followed by 6 nm of chromium or (ii) 3 nm of MoO_x plus 6 nm of chromium. To minimize the thermal stress of C_8-BTBT-C_8 during PVD of the injection layers, all injection materials are deposited in steps of 0.5 nm, followed by a deposition pause of 2 min. It is known that contamination by water during and after fabrication reduces the device performance.[2,8] Thus, prior to deposition of all layers, the devices are heated to 60 °C at 10^{-7} mbar for several hours. Finally, the structures are sealed at a pressure of 10^{-2} mbar with a 300 nm thick layer of parylene N for inhibiting indiffusion of oxygen and water after device fabrication.[18,19]

Details of the setup for time-resolved THz spectroscopy are described in the previous work.[20] Few-cycle THz pulses with a bandwidth of about 2.5 THz are time-resolved by electro-optic sampling.[21] All transmission measurements reported here are performed at the temporal peak of the THz pulses (see Fig. 1).

The relative change in the THz transmission signal $\Delta S/S$ with gate voltage V_g is shown in Fig. 2. At negative V_g, holes are injected into the device, and the transmission decreases due to the Drude response of mobile holes. In contrast, a positive gate voltage does not change the transmission signal, as would be expected if mobile electrons were injected. This suggests that if electrons are injected at all, their Drude response can be neglected. In the case of hole injection, $\Delta S/S$ follows linearly the slope of the applied voltage, but only after a threshold voltage V_{th} is reached. The threshold voltage increases on the timescale of several hours. Within the first hour, the threshold voltage is $V_{1h} = 17$ V. After 5 h, the threshold is $V_{5h} = 26$ V. In the following, we will show that the observed increase in the threshold voltage is caused by ion migration of gold into the C_8-BTBT-C_8. These charged defects lead to the build-up of a polarization field, which must be overcome prior to hole injection, as observed by the increase in the threshold voltage with operation time.

With every modulation cycle, the devices are charged with density $n_{2D,mod}$, which can be deduced from the capacitance per unit area $\tilde{C}$ of the structures. A gate voltage of $V_g = -50$ V and $\tilde{C} = 6.1$ nF/cm^2 leads to $n_{2D,mod} = 1.9 \times 10^{12}$ cm^{-2}. The density of the mobile holes n_{2D} is deduced from the triangular modulation curves in Fig. 2 by considering the delayed onset due to the injection thresholds V_{th}. For the curve recorded after 1 h operation, the sheet density of mobile holes drops to $n_{2D} = 0.7 \times 10^{12}$ cm^{-2}, which is less than 40% of $n_{2D,mod}$. The difference is attributed to the polarization field due to charged defects. Similar values were reported in Ref. 22.

In order to obtain the sheet conductivity of the charge carriers within the device, electromodulation experiments are performed.[15] All data presented in the following are obtained by applying a square wave voltage, for instance, between +50 V and −50 V. For clarity, we describe this modulation by $V_g = -50$ V, because negative bias injects holes into the channel region. Switching the gate voltage V_g changes the density of accumulated holes within the device and, thus, the THz transmission signal S by ΔS. In a good approximation, the sheet conductivity σ_{2D} is related to the relative differential signal as[23]

$$\sigma_{2D} = \frac{-\Delta S}{S} \frac{2\sqrt{\varepsilon_b}}{Z_0}, \quad (1)$$

where Z_0 is the impedance of free space and ε_b is the permittivity of the molecular semiconductor. The sheet conductivity σ_{2D} is extracted from $\Delta S/S$ according to Eq. (1) using $\varepsilon_b = 2.8$.[24,25] Figure 3 shows transients of σ_{2D} for two devices, one with an injection layer of MoO_x and another with a gold injection layer.

Already at the beginning of the measurements shown in Fig. 3, the sheet conductivity of the device with the gold injection layer is strongly reduced compared to the value measured for the MoO_x layer. This observation rules out degradation due to intercalated water and contamination by gases such as oxygen, because the Au/Cr devices as well as the MoO_x/Cr devices were fabricated using similar processes. As shown in Fig. 3, the initial conductivity of the gold devices is smaller than the conductivity of the MoO_x structures, which may be caused by the ingress of gold during deposition.[14] More interesting is that the conductivity with the gold injection layer rapidly decreases, whereas the decay of the MoO_x device is marginal. These differences show that gold migration causes the observed device degradation. The reason for the minor degradation of the MoO_x device is not accessible from the data available.

The THz transmission experiments probe the sheet conductivity of the channel $\sigma_{2D} = e\, n_{2D}\, \mu$, where n_{2D} is the sheet density of mobile holes and μ is their mobility. The answer to the question of whether the observed degradation results from a reduction of n_{2D} or from a reduction of μ cannot be derived from Fig. 4 alone. However, all experiments are performed at a modulation frequency of about 11 Hz. At such low frequencies, the contact resistances only marginally delay the injection and extraction of the holes, and the density of mobile holes is $n_{2D} = \tilde{C}\,(V_g - V_{th})/e$. This yields with Eq. (1) for the mobility

$$\mu = \frac{-\Delta S}{S}\,\frac{2\sqrt{\varepsilon_b}}{Z_0}\,\frac{1}{\tilde{C}\,(V_g - V_{th})}. \tag{2}$$

As shown in Fig. 2 the slopes of $\Delta S/S$ are proportional to $V_g - V_{th}$, too. Thus, μ is constant during degradation, which supports the notion that charged defects cause a polarization field that hinders the injection of mobile holes. Similar conclusions were drawn in Refs. 3 and 15.

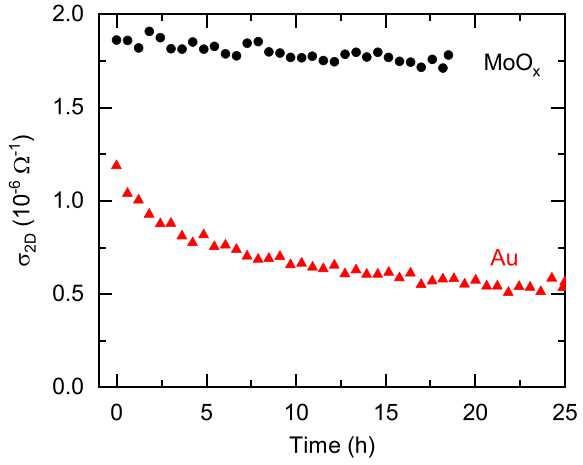

FIG. 3. Change in the sheet conductivity σ_{2D} with time. Data obtained on devices with a gold injection layer and with a MoO_x injection layer are shown by red triangles and black circles, respectively.

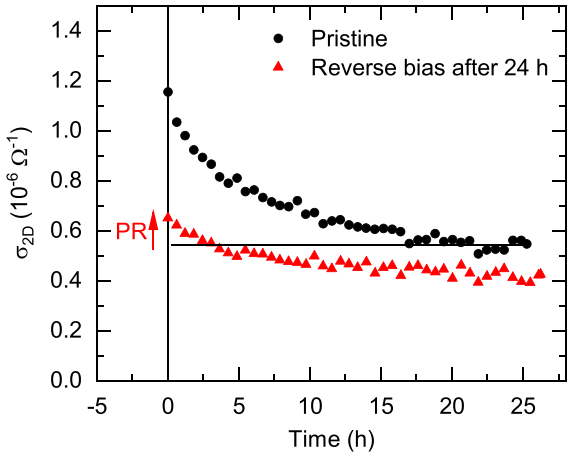

FIG. 4. Decay of the sheet conductivity σ_{2D} with operation time. Dots show the degradation of a pristine sample. Triangles show a repeated measurement on the same structure after a DC reverse bias of $V_{rev} = +50$ V is applied for 24 h. The red arrow indicates the partial recovery (PR).

Figure 4 shows that the mechanism behind the degradation is the field-induced migration of gold out of the injection layer into the semiconductor. Within 20 h, the conductivity σ_{2D} of a pristine device diminishes by about 50%. The device performance, however, can be partially restored by applying a DC reverse voltage of $V_{rev} = +50$ V for 24 h. Apparently, first, the field-induced transport of gold leads to the degradation of the device, and the following application of the reverse bias drives a part of the gold back from the channel region toward the injection layer. Because the electrical field within the device is homogeneous, only charged particles are subject to field-induced transport, which encourages usage of the term ion migration.

Investigating the temperature dependence of device degradation provides further insight.[5,26–28] Figure 5 shows that the degradation

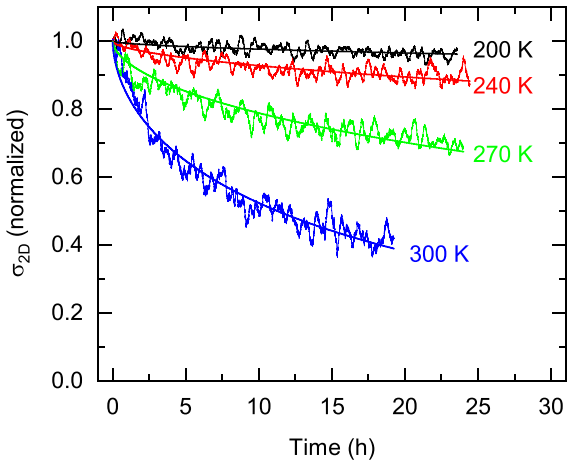

FIG. 5. Decay of the normalized sheet conductivity for different temperatures. Also shown are fits by a stretched exponential according to Eq. (3).

decelerates with decreasing temperature. At $T = 200$ K, a degradation is barely visible within the first 24 h. For quantitative access, the experimental data are normalized and fitted by a stretched exponential[2,3,29]

$$\sigma_{2D}(t) = \sigma_0 \exp\left(-\left(\frac{t}{\tau}\right)^{\beta}\right), \quad (3)$$

with time constant τ and stretching factor β. Fitting the curve for $T = 300$ K provides $\beta = 0.575$. Determining τ along with β is impossible at lower temperatures, because the dynamics become too small. Although the dependence of β on temperature often provides valuable insight into the process of trap formation,[30] we use $\beta = 0.575$ for $T \leq 270$ K, too. The determined time constants range from $\tau = 21$ h to $\tau = 6700$ h for $T = 300$ K and 200 K, respectively.

Figure 6 shows Arrhenius plots of the degradation rate $\gamma = 1/\tau$ obtained at gate voltages V_g of −30 V and −50 V. For all temperatures, the rates obtained at $V_g = -30$ V are about one order of magnitude smaller than those determined for $V_g = -50$ V. Two conclusions can be drawn from this disproportionality: (i) the electric field within the devices is the driving force behind the degradation; (ii) the reactants involved in the degradation process are already abundant before the field-induced degradation begins. Otherwise, the field strength would have only a marginal effect on degradation, because the intake of contaminants would govern the degradation dynamics. This excludes, for instance, the indiffusion of water or oxygen, as can be expected for the studied devices, because they were sealed with parylene. This is also supported by the marginal degradation of the MoO_x device.

Because the observed decays of $\sigma_{2D}(t)$ depend on temperature, the physical processes behind the time constants can be understood to be thermally activated,[31]

$$\tau = \tau_0 \exp\left(\frac{E_\tau}{k_B T}\right), \quad (4)$$

where E_τ is the activation energy associated with τ. Fitting the data of Fig. 4 provides for both gate voltages V_g nearly identical values of $E_\tau(-30\,\text{V}) = 0.291 \pm 0.082$ and $E_\tau(-50\,\text{V}) = 0.293 \pm 0.035$ eV.

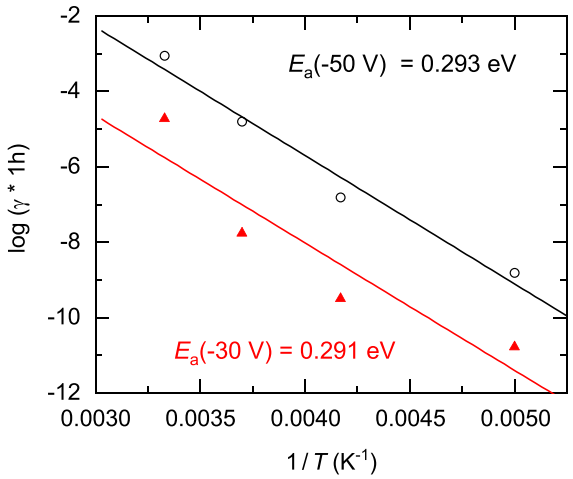

FIG. 6. Dependence of the decay rate $\gamma = 1/\tau$ on inverse temperature $1/T$. The datasets recorded at gate voltages of −30 V and −50 V are shown by triangles and circles, respectively. The solid lines show fits to the experimental data using the indicated activation energies.

From this result, we draw the following picture for migration of gold within the field: on their way toward the channel region, the gold ions are frequently trapped. The gold ions do not overcome the traps' barriers with the help of the driving field; otherwise, the activation energy E_τ would depend on the field strength. Similar activation energies between 0.3 and 0.67 eV were reported for various other organic semiconductors, when gold electrodes were used.[2,26,28,29]

The geometrical dimensions of the semiconductor's lattice cells suggest a transport mechanism for gold that considers trapping and release of the gold ions on their way along the electric field. The unit cell's lattice constants of C_8-BTBT-C_8 perpendicular to the field are $a = 5.927$ and $b = 7.880$ Å.[32] For a guest atom within the lattice, the available volume is further reduced by the second C_8-BTBT-C_8 molecule within the unit cell. Good estimates for the gold's atomic and ionic diameters are $d^0 \approx 4$ and $d^+ \approx 3$ Å, respectively.[33] Although these values were deduced for distinctly different binding environments, it is obvious that the presence of gold leads to a severe deformation of the lattice. The transfer of gold between unit cells requires the target cell to provide the needed space. This lattice deformation requires a thermal activation with which we associate the observed value of $E_\tau \approx 0.29$ eV. An extreme case of how gold changes the geometrical properties of the host material was reported by Grodd *et al.*[12] The authors observed with x-ray diffraction that indiffusion of Au into poly(3-hexylthiophene) leads to the formation of Au nanocrystallites within the host semiconductor. Such colloids are also known for enhancing oxidation in the presence of water and oxygen, for instance, observed on polysilanes.[34]

In conclusion, we reported on THz experiments that map the degradation of molecular field-effect devices due to ion migration of gold during device operation. The charged gold defects reduce the density of mobile holes and their sheet conductivity. Additionally, a polarization field is built up, which increases the threshold voltages with the operation time of the devices. The degradation of the devices strongly depends on the field strength between the injection layer and the gate contact. The deduced activation energies for migration of gold indicate that thermal excitation of lattice deformations of the semiconductor facilitates ion migration. Altogether, the results show that field-induced transport of metals from device contacts is a technological challenge on the way toward reliable FETs of molecular semiconductors.

This research was funded by the Deutsche Forschungsgemeinschaft (DFG, German Research Foundation), Contract No. KE 516/11-1.

AUTHOR DECLARATIONS

Conflict of Interest

The authors have no conflicts to disclose.

DATA AVAILABILITY

The data that support the findings of this study are available from the corresponding author upon reasonable request.

REFERENCES

[1]H. Sirringhaus, Adv. Mater. **21**, 3859 (2009).
[2]S. G. J. Mathijssen, M. Cölle, H. Gomes, E. C. P. Smits, B. de Boer, I. McCulloch, P. Bobbert, and D. M. de Leeuw, Adv. Mater. **19**, 2785 (2007).
[3]P. P. Cielecki, T. Leissner, M. Ahmadpour, M. Madsen, H.-G. Rubahn, J. Fiutowski, and J. Kjelstrup-Hansen, Org. Electron. **82**, 105717 (2020).

[4]J. Tardy and M. Erouel, Microelectron. Reliab. **53**, 274 (2013).
[5]R. A. Street, Phys. Rev. B **77**, 165311 (2008).
[6]S. D. Wang, T. Minari, T. Miyadera, Y. Aoyagi, and K. Tsukagoshi, Appl. Phys. Lett. **92**, 063305 (2008).
[7]C. Goldmann, D. J. Gundlach, and B. Batlogg, Appl. Phys. Lett. **88**, 063501 (2006).
[8]H. L. Gomes, P. Stallinga, M. Cölle, D. M. de Leeuw, and F. Biscarini, Appl. Phys. Lett. **88**, 082101 (2006).
[9]A. Tamayo, T. Salzillo, and M. Mas-Torrent, Adv. Mater. Interface **9**, 2101679 (2022).
[10]A. Benor, A. Hoppe, V. Wagner, and D. Knipp, Org. Electron. **8**, 749 (2007).
[11]T. Hallam, C. M. Duffy, T. Minakata, M. Ando, and H. Sirringhaus, Nanotechnology **20**, 025203 (2009).
[12]L. S. Grodd, E. Mikayelyan, T. Dane, U. Pietsch, and S. Grigorian, Nanoscale **12**, 2434 (2020).
[13]A. C. Dürr, F. Schreiber, M. Kelsch, H. D. Carstanjen, and H. Dosch, Adv. Mater. **14**, 961 (2002).
[14]J. H. Cho, D. H. Kim, Y. Jang, W. H. Lee, K. Ihm, J.-H. Han, S. Chung, and K. Cho, Appl. Phys. Lett. **89**, 132101 (2006).
[15]T. R. Arend, A. Wimmer, G. Schweicher, B. Chattopadhyay, Y. H. Geerts, and R. Kersting, J. Phys. Chem. Lett. **8**, 5444 (2017).
[16]J. B. Fortin and T.-M. Lu, *Chemical Vapor Deposition Polymerization: The Growth and Properties of Parylene Thin Films* (Kluwer Academic Publishers, Boston/Dordrecht/New York/London, 2004).
[17]P. Xie, T. Liu, J. Sun, and J. Yang, Adv. Func. Mater. **32**, 2200843 (2022).
[18]G. W. Hyung, J. Park, J. H. Kim, J. R. Koo, and Y. K. Kim, Solid-State Electron. **54**, 439 (2010).
[19]S. Nair, M. Kathiresan, T. Mukundan, and V. Natarajan, Microelectron. Eng. **163**, 36 (2016).
[20]S. G. Engelbrecht, T. R. Arend, T. Zhu, M. J. Kappers, and R. Kersting, Appl. Phys. Lett. **106**, 092107 (2015).
[21]Q. Wu and X.-C. Zhang, Appl. Phys. Lett. **67**, 3523 (1995).
[22]W. Choi, T. Miyakai, T. Sakurai, A. Saeki, M. Yokoyama, and S. Seki, Appl. Phys. Lett. **105**, 033302 (2014).
[23]S. G. Engelbrecht, M. Prinz, T. R. Arend, and R. Kersting, Appl. Phys. Lett. **105**, 012101 (2014).
[24]C. Grigoriadis, C. Niebel, C. Ruzie, Y. H. Geerts, and G. Floudas, J. Phys. Chem. B **118**, 1443 (2014).
[25]W. Choi, Y. Tsutsui, T. Sakurai, and S. Seki, Appl. Phys. Lett. **110**, 153303 (2017).
[26]D. V. Lang, X. Chi, T. Siegrist, A. M. Sergent, and A. P. Ramirez, Phys. Rev. Lett. **93**, 076601 (2004).
[27]T. Miyadera, S. D. Wang, T. Minari, K. Tsukagoshi, and Y. Aoyagi, Appl. Phys. Lett. **93**, 033304 (2008).
[28]H. Lee, B. Moon, S. Y. Son, T. Park, B. Kang, and K. Cho, ACS Appl. Mater. Interface **13**, 16722 (2021).
[29]H. L. Gomes, P. Stallinga, F. Dinelli, M. Murgia, F. Biscarini, D. M. de Leeuw, T. Muck, J. Geurts, L. W. Molenkamp, and V. Wagner, Appl. Phys. Lett. **84**, 3184 (2004).
[30]S. C. Deane, R. B. Wehrspohn, and M. J. Powell, Phys. Rev. B **58**, 12625 (1998).
[31]L. E. Benatar, D. Redfield, and R. H. Bube, J. Appl. Phys. **73**, 8659 (1993).
[32]H. Kobayashi, N. Kobayashi, S. Hosoi, N. Koshitani, D. Murakami, R. Shirasawa, Y. Kudo, D. Hobara, Y. Tokita, and M. Itabashi, J. Chem. Phys. **139**, 014707 (2013).
[33]*CRC Handbook of Chemistry and Physics*, edited by W. M. Haynes, D. R. Lide, and T. J. Bruno (CRC Press, 2014).
[34]N. Nagayama, T. Maeda, Y. Sakurai, and M. Yokoyama, Mol. Cryst. Liq. Cryst. **316**, 411 (1998).